A Bpp-based Dinuclear Ruthenium Photocatalyst for Visible Light-Driven Oxidation Reactions

Seán Hennessey[a], Pau Farràs[a,b*], Jordi Benet-Buchholz[c], Antoni Llobet[b,c*]

a - School of Chemistry, Energy Research Centre, Ryan Institute, National University of Ireland, Galway (NUI Galway), University Road, H91 CF50 Galway, Ireland.
b - Institute of Chemical Research of Catalonia (ICIQ), Av. Països Catalans 16, 43007 Tarragona, Spain.
c -Departament de Química, Universidad Autònoma de Barcelona, Cerdanyola del Vallès, 08193 Barcelona, Spain.
*Correspondence: pau.farras@nuigalway.ie; Tel.: +353 91 492765 (P.F.); allobet@iciq.es; Tel.: +34 977 920 000 (A.L.)

Abstract

A diruthenium dyad molecule consisting of a 2,2-(1H-pyrazole-3,5-diyl)dipyridine (Hbpp) bridging ligand with the formula out-/in-[(bpy)2Ru(bpp)Ru(L)tpy)]$^{n+}$ (bpy = 2,2′-bipyridine, tpy = 2,2′:6′,2″-terpyridine, L = Cl, CF_3COO^- , H_2O or CH_3CN and n = 2 or 3) has been prepared and fully characterised. The complex has been characterized by analytical and spectroscopic techniques and by X-ray diffraction analysis for two of the derivatives (Cl and CH_3CN). Additionally, full electrochemical characterization based on cyclic voltammetry and square wave voltammetry has been also performed. The pH dependence of the redox couples for the aqua complex has also been studied and the corresponding Pourbaix diagram drawn. Furthermore, the capacity to photo-catalytically oxidize organic substrates, such as alcohols, alkenes, and sulfides, has been carried out and the overall stability and selectivity of the catalyst has been analysed.

1. Introduction

Moving away from the earth's heavy reliance on fossil fuels is one of the greatest challenges facing researchers today.[1] Due to the abundance and cleanliness of the energy source, using solar energy to drive chemical reactions for the production of useful materials and fuels is an attractive alternative to conventional carbon-heavy methods.[2] The area of solar-driven chemistry has become very promising to the scientific community looking at ways of artificial water splitting and green chemistry.[3] The opportunity for industrial-scale processes to use 100% renewable energy in the synthesis of useful chemical material is a highly attractive proposition.[4] Furthermore, removing the necessity of certain reagents in industrial processes that produce by-products that

have a negative environmental impact, such as permanganate and certain metal oxides, is of significant importance.[5] To bypass these difficulties, the implementation of water as an oxygen source can provide an inexpensive and environmentally friendly alternative with a very high atom economy.[6,7]

The production of solar chemicals can be performed using different methods, from purely heterogeneous and homogeneous catalysis to intermediate hybrids in which molecular catalysts are immobilised on semiconducting surfaces. However, many of these systems focus on using a homogenous mixture of a photosensitizer and a (photo)catalyst,[8] which has the negative effect of poor intermolecular electron transfer between the two systems. However, dinuclear systems containing both a photosensitizer and catalyst in a single molecular system have potential to overcome these problems. To achieve this, dinuclear transition metal complexes arrayed in a chromophore-catalyst, or 'dyad', arrangement have been considered as an alternative. These dinuclear species are of particular interest as it has been shown that due to the close proximity of the two metal centres, intramolecular electron transfer is improved in comparison to their mononuclear counterparts.[9] These dyads consist of a photosensitizing light-harvesting unit M_p, and a catalytic centre M_c, to give an overall complex M_pM_c. The use of ruthenium-based polypyridyl complexes has been widely studied in both the applications of photosensitizers and (photo)catalysts.[4] As a result, dinuclear ruthenium complexes have been utilized to give complexes of formula, Ru_pRu_c,[10,11] although other metals and photosensitizing units have also been incorporated with Ru based polypyridyl units.[12,13] These complexes are coupled through a bridging ligand, through which intramolecular electron transfer takes place.

The standout feature of these dyad systems is the molecular electronics as a result of the auxiliary and bridging ligands. These ligands can alter the orbital energy, excited state lifetime and redox potentials of both the Ru_p and Ru_c.[10] The bridging ligand is key to the overall processes of these dyads, as the strength of the bonding of the systems has been studied to proportionally effect the speed of the intramolecular electronics of the system.[14] Previous work performed by Jakubivoka *et al.* looked at the spatial localization of excited state electrons in a variety of chromophore-catalyst assemblies. This work used density functional theory (DFT) to determine the effects of modification of bridging ligands on intramolecular electron transfer in the dyad.[15] Thereby showing

how an extended π-conjugated ligand can shift the electronic excitations effectively from the bridging ligand into the terminal ligand.

By basing choice of ligand on the Robin and Day classification of inner-sphere electron transfer, bridging ligands can be tailored to optimise electron transfer.[16,17] Examples of which are shown in **Error! Reference source not found.**. A class I system, like that shown in **Error! Reference source not found.**a,[18] involves weak electronic interaction between two species in an entirely decoupled independent system. This poor electron transfer can be improved upon by the introduction of a bridging ligand like that seen in **Error! Reference source not found.**b and 1c.[10,19] This class II system contains localized valences (oxidation states) and measurable electronic coupling between the two metal centres, giving rise to two redox sites that are mutually dependent. Work by Chen *et al.*, showed that a very strong electronic coupling through the bridging ligand (in this case a 2,3,5,6-tetrakis(2-pyridyl)pyrazine) results in charge trapping between the chromophore and catalyst centres.[20] This delocalisation of charge was thought to be responsible for the decreased catalytic performance.

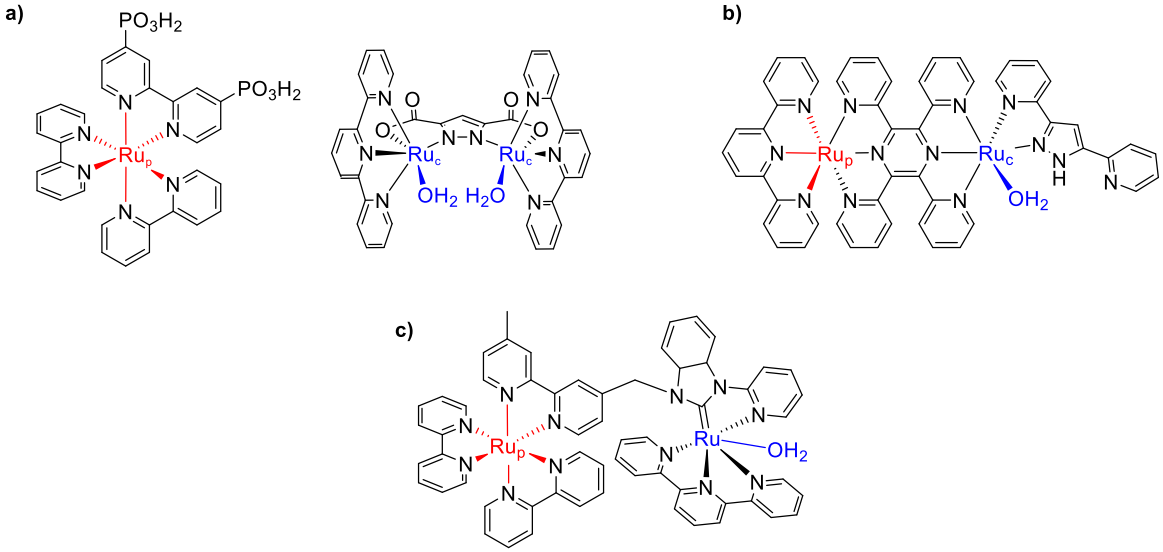

Figure 1: Examples of previous ruthenium polypyridyl systems with photosensitizing, Rup, (red) and catalytic, Ruc, (blue) units highlighted a) unlinked chromophore – catalyst system.18 b) Bridged diruthenium systems through highly decoupled aromatic bridge.[19]

Several examples of dyad systems have already been demonstrated to have high selectivity towards the photocatalytic oxidation of organic substrates such as alcohols, sulfides and alkenes.[10,11,20–24] The higher oxidation states required for the oxidation of these substrates is achieved due to the fast intramolecular electron transfer between the two Ru units.[25] Therefore,

building on this previous work, by using a bridging ligand that enables long-lived charge-separated states, while ensuring good electron transfer can potentially lead to much more efficient catalysis. Herein we investigate the use of the bridging ligand, Hbpp, in the framework of the dyad, *out*-/*in*-[(bpy)$_2$Ru(bpp)Ru(L)(tpy)]$^{n+}$ (L = Cl, CF_3COO^-, H_2O or CH_3CN, n = 2 or 3). We have characterized this dyad by a combination of analytical, photophysical, and electrochemical techniques. Additionally, we have tested the capacity of the dyad for carrying out photoinduced oxidation of organic substrates, such as alcohols, sulfides, alkenes and its water oxidation potential. We have used the data gathered to compare to similar systems used in the photocatalytic oxidation of organics.

2. Results and Discussion

Both synthetic pathways utilized begin with the synthesis of the bridging ligand 2,2-(1H-pyrazole-3,5-diyl)dipyridine (**Hbpp**), as seen in **Scheme 1**. From there, complexation of this ligand with either ruthenium component (Ru_p or Ru_c) is possible. Complexation of the Hbpp with Ru(tpy)Cl_3 leads to the formation of the intermediate mononuclear complex, *out*-[Ru(Cl)(Hbpp)(tpy)]$^{2+}$, ***out*-1^{2+}**.[26] Further reaction of ***out*-1^{2+}** with Ru(bpy)$_2Cl_2$ produces the *out*- isomer of the dyad, *out*-[(bpy)$_2$Ru(bpp)Ru(Cl)(tpy)]$^{2+}$, ***out*-[3-Cl]$^{2+}$**. However, this isomer of the dyad was shown to be highly unstable, a feature which is accelerated by light irradiation. This instability is observed by a noticeable colour change from red to purple over short time periods as well as noticeable changes in the UV-Vis spectroscopy (**Error! Reference source not found.2**) and cyclic voltammetry (Figure S1). The degradation of an impure sample has also been observed *via* ^{1}H-NMR spectroscopy (Figure S2). The UV-Vis of ***out*-[3-Cl]$^{2+}$** shows bands mainly corresponding to that of the Ru_p unit, Ru(bpy)$_2$.

The Ru_c centre formed from ***out*-1^{2+}** has a weak ε value similar to other Ru-Cl complexes, resulting in these bands showing very weakly in the 400-600 nm region of ***out*-[3-Cl]$^{2+}$**.[26] The product obtained after light degradation is similar to that of the free Ru(bpy)$_2Cl_2$, based on the UV-Vis, suggesting that this is reformed after degradation. This is supported both by the colour change (as Ru(bpy$_2$)Cl_2 is a distinct purple colour) and by the CV of the degraded species, which appears to show the reformation of Ru(bpy)$_2Cl_2$ in addition to the appearance of several new peaks. These further peaks suggest the formation of several individual Ru-based species, which were not distinguishable in the UV-Vis. This is also supported by the NMR, which suggests the

reformation of ***out*-1**$^{2+}$ after light irradiation. It is theorized that the *out*- isomer is disfavoured due to the geometric constraints between the tpy and bpy of the two respective Ru units of the dyad.

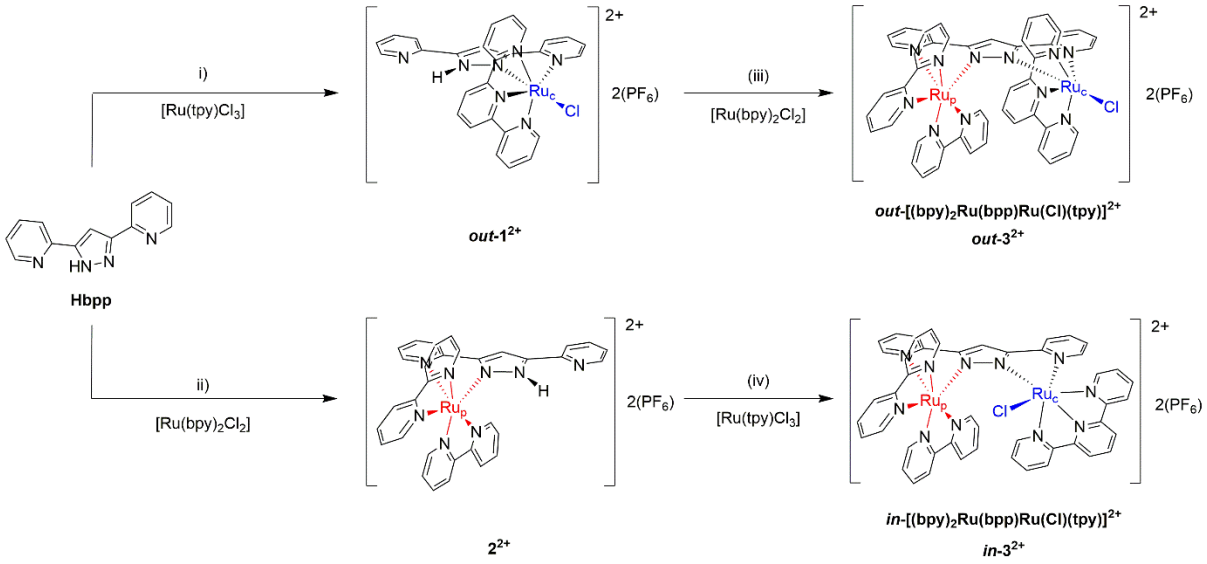

Scheme 1: Two possible synthesis pathways of the two isomers of the Ru dyad. (i) MeOH, 40 °C, overnight, NH_4PF_6 (aq) (ii) EtOH, reflux, 2 hr, NH_4PF_6 (aq) (iii) NEt_3, MeOH, 3 hr, reflux, dark, NH_4PF_6 (aq) (iv) NEt_3, MeOH, 3 hr, reflux, dark, NH_4PF_6 (aq).

With further light excitation the isomerization of the complex to the more favourable *in*- isomer is therefore not feasible, resulting in the relatively rapid degradation of the complex, the speed of which is clearly accelerated by light irradiation based on the quicker degradation in the UV-Vis. To show this, DFT calculations were performed on ***in*-[3-Cl]**$^{2+}$, ***out*-[3-Cl]**$^{2+}$, ***in*-[3-CH$_3$CN]**$^{3+}$, ***out*-[3-CH$_3$CN]**$^{3+}$, and show a clear stabilisation of the *in*- isomers in both cases (see SI), and show no available rotation in the complexes. For the chlorido complexes the energy difference is more pronounced, with the *in*- complex exhibiting a stability of 9.3 kcal/mol over the *out*- counterpart. The difference becomes less important for the acetonitrile complexes, in which the *in*- isomer is 1.9 kcal/mol more stable. However, in both cases the geometries of the complexes in which the tpy and bpy ligands and very close together show that the only way to see isomerism from the *out*- to *in*- isomer would be through bond breaking in the complex, with a concomitant very high activation barrier.

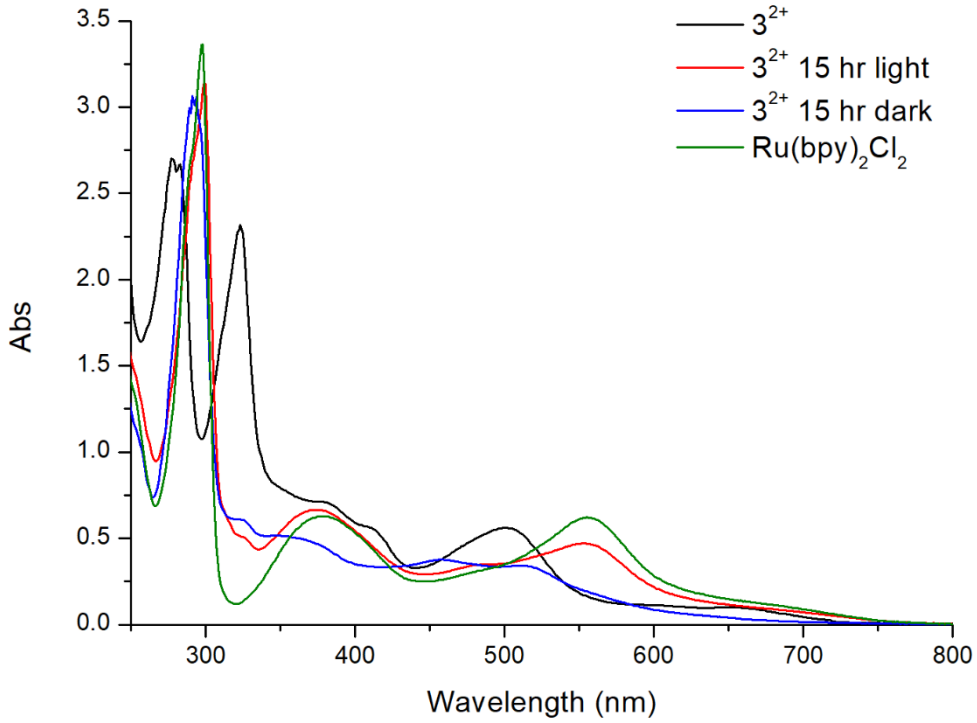

Figure 2: UV-vis absorbance spectra showing degradation of out-[3-Cl]$^{2+}$ in CH_2Cl_2 after 15 h of light irradiation (red). A comparative study of the dyad after 15 h in the dark (blue) is also shown. $Ru(bpy)_2Cl_2$ is shown (green) for comparison.

The *in*-isomer of the dyad, ***in*-[3-Cl]$^{2+}$**, can be synthesized *via* the formation of the intermediate mononuclear complex, $[Ru(Hbpp)(bpy)_2]^{2+}$, **2^{2+}**.[27] From here, further complexation with $[Ru(tpy)Cl_3]$ in excess (12 eq.) of triethylamine leads to the formation of the *in*-dyad. The final reaction mixture, when analysed by mass spectrometry, is shown to contain the dyad, as well as the starting material, **2^{2+}**, and a $Ru(tpy)_2$ complex formed as a side product. To obtain the chloro derivative, successive recrystallisation of the crude reaction using an acetone-diethyl ether mixture leads to the isolation of ***in*-[3-Cl]$^{2+}$** in a 24% yield. The chlorido ligand has been shown to be highly labile with aqua, trifluoroacetate and acetonitrile moieties replacing it readily. We note a clear difference between the *out*- and *in*-isomers in the ^{1}H-NMR (Figure S3). For the *out*- isomer, a doublet appears at 9.90 ppm, while for *in*- isomer, the most downfield signal is at 9.50 ppm. This main difference is attributed to the interaction of the pyridine substituent in the bpp ligand interacting with the Cl of the *out*-isomer, which it is unable to do with the *in*- counterpart.

The dyad can also be separated effectively using semi-preparative HPLC with a acetone:water:trifluoroacetic acid eluent (50:50:0.1) (The HPLC chromatograms and relevant mass spectrometry data are shown in the SI). After drying of the HPLC

fractions, the desired product is shown by mass spec to be ***in*-[3-OOCCF$_3$]$^{2+}$**, with a trifluoroacetate coordinated to the Ru_c unit, as opposed to the chlorido, in a moderate 29% yield. When dissolved in water, the labile ligand position is shown to be in equilibrium between the CF_3COO^- and the OH_2 species, as observed *via* mass spectrometry and ^{1}H-NMR. In d_6-acetone, broad peaks are observed due to the competing equilibrium of the two ligands and their interaction with the ruthenium centre. This competition can also be observed in the ^{19}F-NMR, the individual spectra of which are in the supporting information. The NMR of ***in*-[3-OH$_2$]$^{3+}$** in D_2O show the two PF_6 signals at -71.32 and -73.20 ppm respectively (Figure S4a). However, when performed in acetone-d_6 (Figure S4b) we see the expected upfield shift of the two PF_6 ions due to the different solvent, but in addition we see the appearance of a third peak at -77.73 ppm indicating the presence of the trifluoroacetate ligand bound to the dyad.

2.1. X-Ray Crystallography

Two crystal structures of the Ru dyad have been obtained, with the acetonitrile and chloro ligand bound to the Ru centre (**Error! Reference source not found.a** and **b**). It is possible to obtain the acetonitrile derivative by dissolving up a sample of either ***in*-[3-OH$_2$]$^{3+}$** or ***in*-[3-Cl]$^{2+}$** in acetonitrile, drying, and crystalizing by slow evaporation of a saturated acetone:water solution. On the other hand, it is possible to obtain the ***in*-[3-Cl]$^{2+}$** dyad by successive recrystallization of the final reaction mixture using an acetone-diethyl ether mixture *via* a slow diffusion method. The crystallographic data for the two structures is gathered and shown in Table S1. In the cases of both crystals the cell unit contains two enantiomers which haven't been separated. Both crystal structures present a distorted octahedral geometry around the Ru_c centre, with the tpy in each case occupying the meridional plane, and the bpp ligand coordinating *via* two nitrogen atoms, N6 and N7, as the bridging ligand. The final coordination position contains the acetonitrile or chloro ligand facing the Ru_p unit. The bond distance between the coordinating atom and the Ru_c does vary with the type of ligand group. However, the bond lengths and angles of the Ru-L (Ru-Cl: 2.040 Å, Ru-$NCCH_3$: 2.407 Å) are similar to that of previous Ru complexes in the literature.[10,28] The geometry of the Ru_p unit is fairly unremarkable and contains the $Ru(bpy)_2$ unit in the commonly observed *cis*-fashion in both cases.

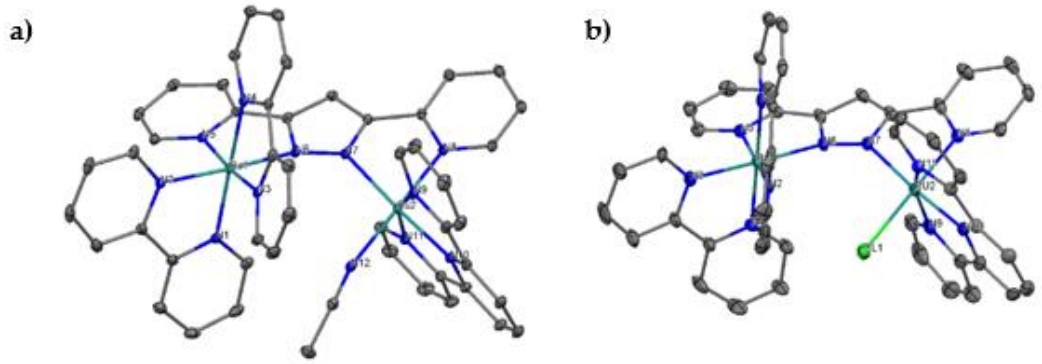

Figure 3 Single-crystal X-ray structure of a) ***in*-[3-CH_3CN]$^{3+}$** (thermal ellipsoid plot drawn at 30% probability). b) ***in*-[3-Cl]$^{2+}$** (thermal ellipsoid plot drawn at 20% probability). All hydrogens, hexafluorophosphate counterions and solvent molecules (acetone) have been omitted for clarity

2.2. Spectroscopic Properties

The dyad, ***in*-[3-$OOCCF_3$]$^{2+}$**, is fully characterized by both 1D and 2D NMR, the spectra of which are shown in the supporting information. The chloro and acetonitrile derivatives have also been characterized by ^{1}H-NMR and ^{13}C-NMR (See SI) as well as testing their photophysical and electrochemical properties. The photophysical characterization of the aqua derivative has been performed by UV-Vis, the spectra of which is shown in **Error! Reference source not found.**. Three main regions can be distinguished from the UV-vis spectroscopy. The distinct bands observed between 250 and 400 nm correspond to the intra-ligand π–π* transitions that arise as a result of the high aromaticity of the bpy, tpy and bpp ligands. The broad band detected between 400 and 540 nm is assigned to the unsymmetrical Ru(dπ)-tpy/bpy/bpp(π*) metal-to-ligand charge transfer (MLCT) bands. The last significant band is the broad region between 540 and 620 nm, in which d-d transitions are known to be common (highlighted *via* inset in **Error! Reference source not found.**). The UV-Vis redox titration of the aqua complex was studied by the subsequent addition of 1 eq. of the oxidant cerium (IV) ammonium nitrate (CAN), from which the spectra of the different oxidized species formed can be observed, which is shown in **Error! Reference source not found.a** (the slower additions of 0.1 eq. of CAN is shown in Figure S5). As has been seen in previous cases, the appearance of a band at 600 nm is due to the production of an Ru_c^{IV}=O

complex as a result of the oxidation of the dyad.[29] In addition, we observe a significant decrease in the MLCT absorption band at 450 nm after the addition of 1 equivalent of oxidant, which is further oxidized by two additional equivalents of CAN. This is followed up by the complete disappearance of the band upon the addition of the 4th equivalent of CAN, indicating oxidation of the Ru_p^{II} to Ru_p^{III} species. This is further proven by the significant increase in absorption at 600 nm, which corresponds to the formation of the Ru_p^{III} species after the final addition of CAN.

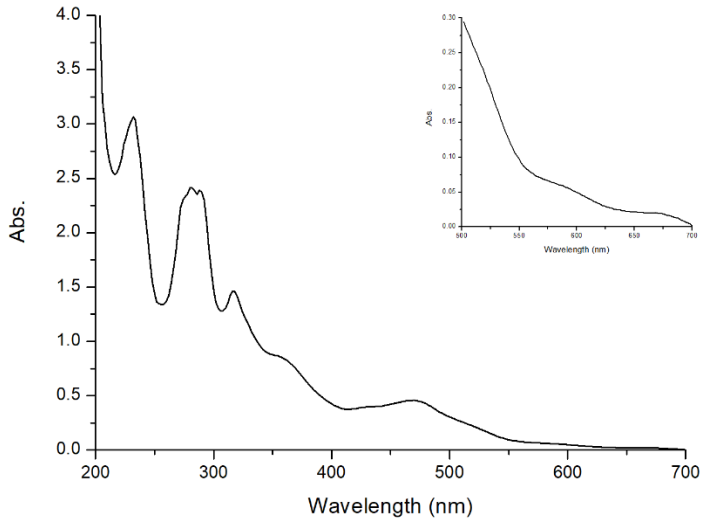

Figure 4: The UV-vis absorbance spectra for in-[3-OH_2]$^{3+}$ in CF_3SO_3H at pH = 1. Transitional d–d absorption band between 500–700 nm shown inset for clarity.

The stability of the aqua complex was tested by addition of the oxidant CAN. Upon the addition of 1 equivalent of the oxidant in Error! Reference source not found.**b** we notice a sizeable decrease in the MLCT band as a result of the oxidation of the Ru_c^{II}-OH_2/Ru_c^{III}-OH. After the addition of 1 eq. of CAN, the dyad was left for 900 mins to determine the stability of the Ru_c^{III}-OH species. The spectrum observed after this time period indicate that the initial species is not reformed, indicating a change in structure, although we do observe the band at 600 nm return, suggesting the presence of some recovered Ru_c^{II}. Due to the need for robust catalysts the stability of the complex over a range of pH was tested to determine its feasibility under different reactions conditions. To test the robustness, the dyad was exposed to a harsh environment (pH = 12, Ru_c^{II}-OH) and exposed to air in the absence of any organic substrate and monitored by UV-Vis spectroscopy (Figure S6). No significant change in the UV-Vis was observed over time, suggesting good stability of the complex, with the decreasing MLCT over the time

period being attributed to the precipitation of the dyad and subsequent decreased concentration.

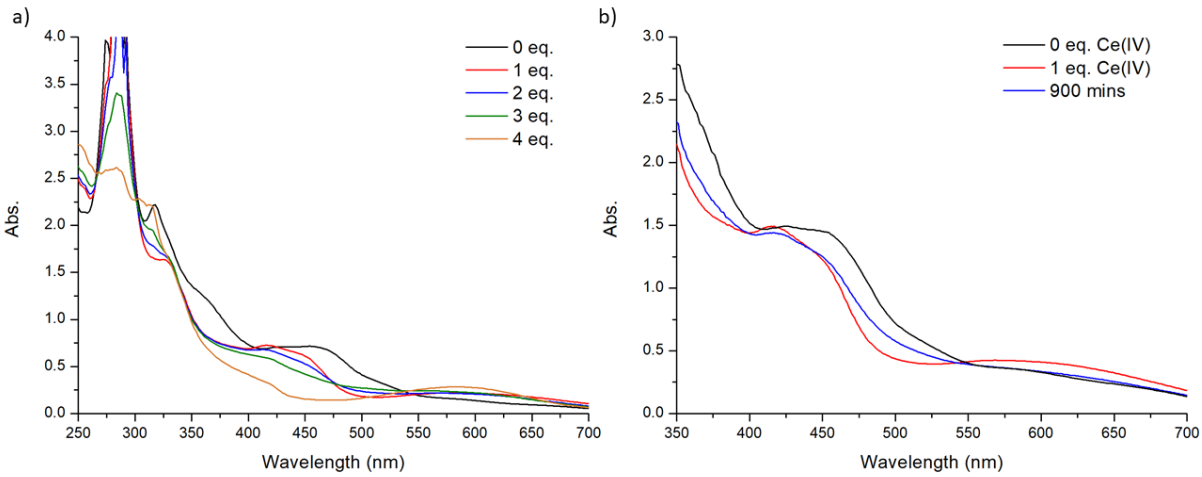

Figure 5: UV-vis absorbance spectra of oxidized products of in-[3-OH_2]$^{3+}$ upon addition of 1 to 4 equivalents of Ce(IV) under air in 0.1 M CF_3SO_3H (pH = 1). **5b**: UV-vis absorbance spectra of in-[3-OH_2]$^{3+}$ (black line), in-[3-OH_2]$^{3+}$ with 1 eq. of Ce(IV) (red line) and after 900 min exposed with 1 eq., all in 0.1 M CF_3SO_3H.

A key aspect of this work is the structure/activity relationship affected by the bridging ligand in dinuclear ruthenium dyads. As discussed in the introduction, Hbpp is a weak bridging ligand. But as a comparative study there was a necessity to compare the ligand strength with that of other similar reported ligands. Therefore, to quantify the value the delocalization energy (H_{ab}), the electronic coupling between the donor and acceptor of a coupled redox site was used, this is related to the integrated absorption band intensity, and its relationship is given by equation 1;

$$H_{ab} = \frac{2.05 \times 10^{-2}}{r} \left(\varepsilon_{max} \bar{\nu}_{max} \Delta\bar{\nu}_{1/2}\right)^{\frac{1}{2}} \qquad \textbf{(1)}$$

Where ε_{max} is the molar absorptivity coefficient, $\bar{\nu}_{max}$ is the absorption maximum in cm^{-1}, $\Delta\bar{\nu}_{1/2}$ is the width at half the height in cm^{-1} and r is the distance between the two Ru centers in angstroms.[30] From the NIR spectra (Figure S7) and crystal structure data we can characterize the electronic coupling of the bridging ligand). Under the Robin and Day classification, a class I complex has a $H_{ab} = 0$, with class II arising from $0 < H_{ab} < \lambda/2$), and class III arising when $2H_{ab}/\lambda \geq 1$.[31,32] In the case of the dyad analyzed herein, the ε_{max} of 170.6 $M^{-1}cm^{-1}$ at a wavelength of 8422 cm^{-1} we obtain a value of 184.6 cm^{-1} for H_{ab}, indicating that the dyad is a class II system. The small value of H_{ab} suggests that the dyad, ***in*-[3-OH_2]$^{3+}$** is on the weak side of class II complexes. The equations corresponding to each electrochemical transition are shown below.

At pH = 7:

$$Ru_p^{II}Ru_c^{III}\text{-}OH + 1e^- \rightarrow Ru_p^{II}Ru_c^{II}\text{-}OH_2 \quad \textbf{(2)}$$

$$E_{1/2}° = 0.412\ V$$

$$Ru_p^{II}Ru_c^{IV}{=}O + 1e^- + 2H^+ \rightarrow Ru_p^{II}Ru_c^{III}\text{-}OH \quad \textbf{(3)}$$

$$E_{1/2}° = 0.481\ V$$

$$Ru_p^{III}Ru_c^{IV}{=}O + 1e^- \rightarrow Ru_p^{II}Ru_c^{IV}{=}O \quad \textbf{(4)}$$

$$E_{1/2}° = 0.879\ V$$

At pH = 1:

$$Ru_p^{II}Ru_c^{III}\text{-}OH_2 + 1e^- \rightarrow Ru_p^{II}Ru_c^{II}\text{-}OH_2 \quad \textbf{(5)}$$

$$E_{1/2}° = 0.618\ V$$

$$Ru_p^{III}Ru_c^{IV}{=}O + 1e^- + 2H^+ \rightarrow Ru_p^{II}Ru_c^{III}\text{-}OH_2 \quad \textbf{(6)}$$

$$E_{1/2}° = 0.880\ V$$

As is shown by the drawn Pourbaix diagram, at pH = 1, the $Ru_p^{II}Ru_c^{III}\text{-}OH_2$ is present and is further oxidised to the $Ru_p^{III}Ru_c^{IV}{=}O$ species. Of relevance is the $1e^-/2H^+$ transfer leading to very reactive and unstable species (see eq. 4 and eq. 6) observed in other Ru_p^{III} complexes [10]. At pH 7 we observe the formation of a $Ru_p^{II}Ru_c^{III}\text{-}OH$ species across a very narrow potential window, with a significant driving force for Ru_p^{III} to oxidise Ru_c to its active catalytic state, $Ru_c^{IV}{=}O$, which is able to oxidise organic substrates.

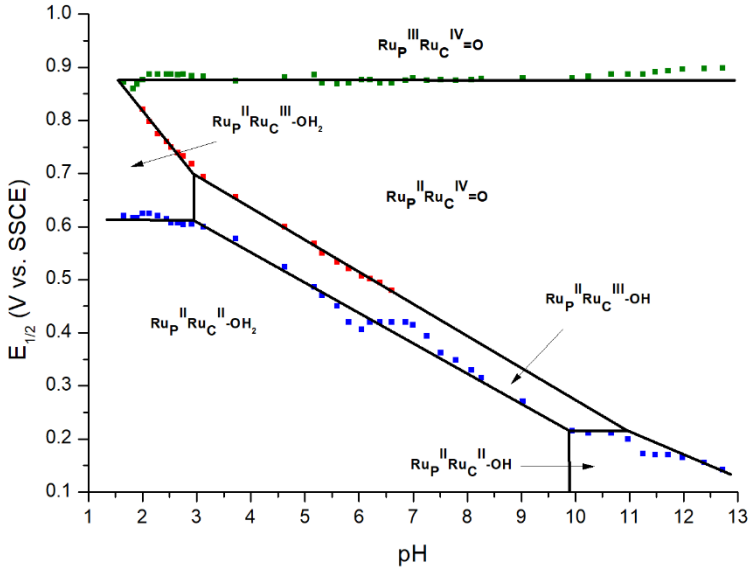

Figure 6: Pourbaix diagram for **in-[3-OH_2]$^{3+}$**. The stability zones of the different species as a function of pH and $E_{1/2}$ (vs. SSCE) are shown and are indicated by the oxidation state of the ruthenium metal and the degree of protonation of the initial aqua group.

The CV experiments displayed in **Figure 7** show the electrocatalytic nature of ***in*-[3-OH$_2$]$^{3+}$** in the presence of increasing concentrations of BzOH. There is a noticeable shift (inset) around 0.9 V as a direct result of oxidation of the alcohol with concomitant reduction of Ru_c^{IV}=O to Ru_c^{III}-OH. This electrochemical change has been observed in previous Ru dyad systems, displaying the fact that the electrocatalytic peak required for the oxidation of the BzOH species begins at this point.[10]

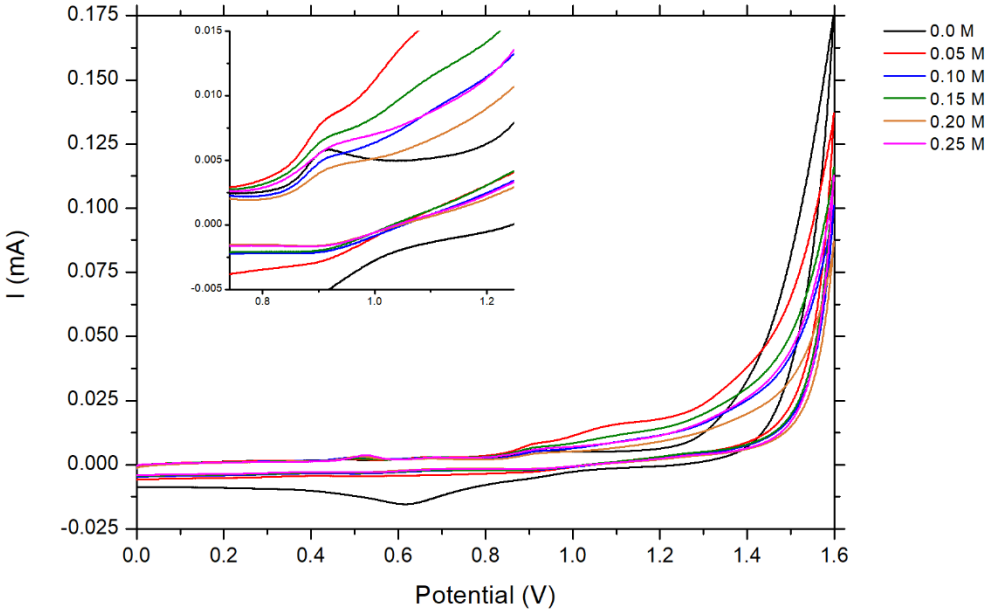

Figure 7: Cyclic voltammograms of **in-[3-OH$_2$]$^{3+}$** (1.0 mM) at pH 1.0 with n Bu_4NPF_6 (0.1 M) supporting electrolyte (scan rate 0.01 V s^{-1}) in a deoxygenated 0.1 M solution of triflic acid after the gradual additions of 0.05 M of BzOH. A zoomed region between 0.70 – 1.30 V is shown inset.

2.3. Photocatalytic Properties

The photocatalytic experiments were all performed by exposing a sealed reaction vial to simulated visible-sunlight irradiation ($\lambda > 400$ nm) for 24 h at room temperature. The samples contained 5 mL of deoxygenated aqueous solutions at pH 7.0 (50 mM phosphate buffer) containing 20 µM ***in*-[3-OH$_2$]$^{3+}$**, 10 mM substrate and 20 mM electron acceptor ($[Co(NH_3)_5(Cl)]Cl_2$). The reaction products were characterized and tracked by ^{1}H-NMR spectroscopy, with yields arising from quantitative analyses of the integrated signal corresponding to the individual reference/substrate, the results of which are displayed in Error! Reference source not found.. The dyad was shown to display a high selectivity for the photocatalytic oxidation of benzyl alcohol, with no overoxidation and formation of carboxylic acid observed, with a turnover number (TON) of 34. This lack of overoxidation was also observed with the sulfide oxidation, with no sulfone present

after catalysis. However, in the case of styrene, due to the low conversion yield, the disappearance of the substrate by NMR is the only quantitative analysis possible, as the products of the photocatalysis were not able to be isolated. The dyad has also been tested under the same conditions without the presence of the organic substrate to determine its light-driven water oxidation properties. However, no O_2 evolution could be seen under the same photocatalytic conditions.

Table 1: Photocatalytic oxidation of organic substrates using **in-[3-OH_2]$^{3+}$** in aqueous solution with comparative values from similar systems. [a]

Catalyst	Substrate	pH	*t* [h]	*T* [°C]	TN[b] (Conv. [%])	Ref.[c]
***in*-3^{3+}**	BzOH	7.0	24	25.0	34 (6.8)	tw
	PhSMe	7.0	24	25.0	103 (20.6)	tw
	4-HSS[d]	7.0	24	25.0	13 (2.6)	tw
A[e]	BzOH	7.0	24	25.0	7 (1.4)	10.
	PhSMe	7.0	24	25.0	67 (13.4)	10.

a - Reaction conditions: deoxygenated aqueous solution, phosphate buffer (50 mM), Catalyst (0.02 mM), substrate (10 mM), $[Co(NH_3)_5Cl]^{2+}$ (20 mM), Xe lamp source (150 W – cut-off filter 400 nm). b - TN = Turnover number. c - tw = this work. d - Protonated form of sodium 4-styrene sulfonate. e - $(tpy)Ru(\mu\text{-}tppz)Ru(OH_2)(bpy)]^{3+}$.

3. Materials and methods

3.1. Materials

Ruthenium trichloride trihydrate was supplied by Alfa Aesar and was used as received. Trifluoromethanesulfonic acid (+99%) was purchased from STREM/CYMIT. Ceric ammonium nitrate, 2,2′- bipyridine, terpyridine, potassium hexafluorophosphate, tetrabutylammonium hexafluorophosphate, ammonium hexafluorophosphate, silver perchlorate, benzyl alcohol, 4-styrene sulfonic acid, phenyl methyl sulfide, pentaamminechloridocobalt(III) dichloride and all organic solvents used were of the highest purity commercially available and were used as received from Aldrich or Acros/Fisher. All solvents were dried prior to use. Aqueous solutions were prepared by using deionized water from an Ultra Clear water purifier system from SG Wasseraufbereitung und Regenerierstation GmbH (conductivity at 25 °C = 0.055 μS cm^{-1}). The compounds Hbpp,[34] $[Ru(tpy)Cl_3]$,[35], *out*-[Ru(bpp)(tpy)Cl] (***out*-1^{2+}**),[26] $[Ru(bpy)_2Cl_2]$,[36] and $[Ru(bpp)(bpy)_2]$ (**2^{2+}**)[27] were all prepared using literature procedures. All synthetic manipulations were routinely performed under a dry dinitrogen atmosphere by using standard Schlenk and vacuum-line techniques.

3.2. Synthesis

Synthesis of out-[3-Cl]$^{2+}$, out-[(bpy)$_2$Ru(bpp)R(Cl)tpy)]$_2$(PF$_6$). In a dark environment, **out-1^{2+}** (100 mg, 0.113 mmol) was mixed with sodium methoxide (13.4 mg, 0.248 mmol, 2 eq.) in 50 mL dry MeOH. The mixture was stirred at rt under N_2 for 30 min. Ru(bpy)$_2$Cl$_2$ (66 mg, 0.136 mmol, 1.2 eq.) was added with a further 80 mL MeOH and refluxed for 3.5 h. The bright red mixture was cooled, solvent removed and dissolved in 10 mL of H_2O/MeOH (4/1). A saturated solution of NH_4PF_6 was added and the red-brown precipitate formed was filtered and isolated. No further purification was carried out due to instability.

Synthesis of in-[3-OOCCF$_3$]$^{2+}$, in-[(bpy)$_2$R(bpp)Ru(OOCCF$_3$)(tpy)] 3(PF6). In a dark environment, Ru(tpy)Cl$_3$ (23.7 mg, 0.054 mmol) was dissolved in 20 mL of dry MeOH under N_2 and dry NEt$_3$ (23 μL, 0.324 mmol, 6 eq.) was added. In a separate flask, [Ru(bpp)(bpy)$_2$]$_2$(PF6) (50 mg, 0.054 mmol) was dissolved in 20 mL of dry MeOH under N_2 and dry NEt$_3$ (23 μL, 0.324 mmol, 6 eq.) was added. The two solutions were stirred at room temperature for 30 min, then combined and refluxed for 2.5 h. The reaction was cooled, and the solvent removed, and the red precipitate dissolved in 10 mL of H_2O/ MeOH (4/1). A saturated solution of NH_4PF_6 was added and the red precipitate formed was filtered and isolated. The title compound was isolated as red microcrystals via a semi-prep HPLC using a acetone:water:trifluoroacetic acid (50:50:0.1) eluent (29% yield). ^{1}H NMR (500 MHz, (CD$_3$)$_2$CO) δ: 9.10 (d, *J* = 5.8 Hz, 1H), 8.97 (d, *J* = 8.1 Hz, 1H), 8.82 (dd, *J* = 16.5, 8.2 Hz, 2H), 8.70 (dd, *J* = 17.5, 8.1 Hz, 2H), 8.62–8.55 (m, 3H), 8.48–8.41 (m, 1H), 8.36–8.30 (m, 1H), 8.28 (s, 1H), 8.27–8.07 (m, 6H), 7.99 (dd, *J* = 15.5, 6.8 Hz, 2H), 7.92 (t, *J* = 6.2 Hz, 2H), 7.78–7.59 (m, 7H), 7.49–7.41 (m, 2H), 7.38 (dd, *J* = 7.5, 5.7 Hz, 1H), 7.34 (dd, *J* = 7.5, 5.8 Hz, 1H), 7.27 (d, *J* = 5.8 Hz, 1H), 7.17 (t, *J* = 7.5, 5.9 Hz, 1H), 6.88 (dd, *J* = 7.4, 5.9 Hz, 1H). ^{13}C NMR (126 MHz, (CD$_3$)$_2$CO) δ: 162.33, 161.90, 160.43, 160.21, 159.58, 159.26, 158.28, 158.19, 156.80, 156.77, 156.36, 155.84, 155.58, 155.03, 154.44, 153.67, 152.45, 151.87, 150.89, 150.82, 150.65, 137.81, 137.57, 137.38, 136.44, 136.26, 135.78, 135.48, 134.12, 127.76, 127.49, 127.13, 126.56, 126.42, 125.59, 124.29, 123.83, 123.71, 123.65, 123.49, 123.14, 123.00, 122.51, 121.76, 121.11, 119.66, 115.46. MS (ESI): 541.4 (M3+). HR-MS (EA): $C_{50}H_{36}F_{15}N_{11}O_2P_2Ru_2$, found: C, 38.5; H, 2.5; N, 10.6. Calc C, 43.69; H, 2.64; N; 11.21.

3.3. Instrumentation and measurements

UV-Vis spectroscopy was performed on a Cary 50 (Varian) UV-Vis spectrophotometer in 1 cm quartz cuvettes. HPLC analysis was performed using a Waters semipreparative chromatograph (up to 40 mL/min) equipped with a 600E multisolvent delivery pump, a Rheodyne 7725i injection valve and 2487 detector. The NMR spectroscopy experiments were performed on a Bruker Avance 400 Ultrashield NMR spectrometer. Samples were run in $CDCl_3$, CH_3OD, D_2O, or $(CD_3)_2CO$ with internal references (residual protons). Elemental analysis was performed by using an EA-1108, CHNS-O elemental analyzer from Fisons Instruments. ESI-MS analyses were recorded on an Esquire 6000 ESI ion trap LC/MS (Bruker Daltonics) instrument equipped with an electrospray ion source. CV and SQWV experiments were performed in a IJ-Cambria IH-660C potentiostat by using a three-electrode cell. A glassy carbon electrode (2 mm diameter) was used as the working electrode, platinum (2 mm diameter) as the auxiliary electrode, and SSCE as a reference electrode. Working electrodes were polished with 0.05 μm alumina paste and washed with distilled water and acetone followed by blow-drying before each measurement. All cyclic voltammograms presented herein were recorded in the absence of light and inside a Faradaic cage. The complexes were dissolved either in CH_2Cl_2 or CH_3CN containing the necessary amount of $^nBu_4NPF_6$ as a supporting electrolyte to yield a 0.1 M ionic strength solution. In aqueous solution, the electrochemical experiments were carried out in 0.1 M CF_3SO_3H (pH 1.0). $E_{1/2}$ values reported herein were estimated from CV experiments as the average of oxidative and reductive peak potentials (where [$E_{1/2}$ = (Ep,a + Ep,c)/2)]) or taken as E(Imax) or SQWV measurements. For construction of the Pourbaix diagrams, the following buffers were used: dihydrogen phosphate/phosphoric acid up to pH 4 (pKa = 2.12), hydrogen phosphate/dihydrogen phosphate up to pH 9 (pKa = 7.67), hydrogen phosphate/sodium phosphate up to pH 13 (pKa = 12.12), sodium hydroxide for pH 14, and 0.1 M triflic acid was used for pH 1.0. The concentration of the species was approximately 1 mM. Oxygen generation in solution was measured by using a water-jacketed Clark electrode reactor from Hansatech. In a typical experiment, a 1.0 mM solution of the complex in CF_3SO_3H (2 mL, pH 1.0) was degassed with nitrogen until no oxygen could be detected. Chemical redox spectrophotometric titrations were performed by sequential addition of a small volume of a solution of Ce^{IV} in CF_3SO_3H (pH 1.0, 50 mL/redox equivalent) to the solution of complex (2.5 mL) in standard 1 cm quartz cuvettes. All density functional

methods calculations were performed in the Gaussian 16 suite of programs[37] by using the M06 functional[38] and an ultrafine integration grid (99 590) in conjugation with the all-electron 6-31G(d) basis set for C, H, N, O, and Cl atoms.[39] The Stuttgart relativistic effective core potential basis set is used for Ru (ECP28MWB).[40,41] All four structures were fully optimized in the gas phase and verified as local minima through frequency calculations.

Kinetics: Experiments were performed on a Cary 50 spectrophotometer equipped with a temperature-controlled cell holder. In a typical experiment, a solution of Ce^{IV} (1 eq) in CF_3SO_3H (10 mL, pH 1.0) was added at 25 °C to a solution of ***in*-[3-OH$_2$]$^{3+}$** (3 mL, 0.1 mM) in 0.1 M CF_3SO_3H.

Light-driven catalytic oxidations: In a typical experiment, a water-jacketed cell containing a deoxygenated aqueous (H_2O, 5 mL) solution at pH 7.04 (50 mM phosphate buffer) with Ru catalyst (0.02 mM), substrate (10 mM), and $[Co(NH_3)_5(Cl)]Cl_2$ (acceptor, 20 mM) was exposed to simulated sunlight (l > 400 nm, UV cut off filter) for 24 h at 25 °C; during which period the mixture was kept under magnetic stirring. Throughout these photocatalytic experiments, visible-light irradiation was provided by a 150 W Xe arc lamp. The incident irradiance at the surface of the reaction vessel was approximately 0.3 W cm^2. The reaction product was characterized by ^{1}H-NMR spectroscopy through quantitative analyses of integrated signal intensities relative to the corresponding reference/substrate. For water oxidation experiments, oxygen generation in solution was measured by using a water-jacketed Clark electrode reactor from Hansatech (2 mL solution).

X-ray crystal structure determination: The crystal complex of ***in*-[3-CH$_3$CN](3PF$_6$)** was obtained dissolving up a sample of the Cl ligand in acetonitrile, drying, and crystalizing using a water:acetone (1:1) mixture with a slow evaporation method. ***in*-[3-Cl](2PF$_6$)** was obtained by a successive recrystallization of the final reaction mother liquor using an acetone-diethyl ether mixture in a slow diffusion process. The measured crystals were prepared under inert conditions immersed in perfluoropolyether as a protecting oil for manipulation.

Data collection: Crystal structure determinations were carried out by using a Bruker-Nonius diffractometer equipped with an APPEX 2 4K CCD area detector, a FR591 rotating anode with MoKa radiation, Montel mirrors as the monochromator, and an Oxford Cryosystem plus low-temperature device (T = -173 °C). Full-sphere data

collection was used with w and f scans. Programs used: Data collection APEX-2,[42] data reduction Bruker Saint V/.60A [43], and absorption correction SADABS.[44]

Structure solution and refinement: Crystal structure solution was achieved by using direct methods as implemented in SHELXTL[45] and visualized by using the program XP. Missing atoms were subsequently located from difference Fourier synthesis and added to the atom list. Leastsquares refinement on F2 by using all measured intensities was carried out with the program SHELXTL. All non-hydrogen atoms were refined, including anisotropic displacement parameters. CCDC-1950948 (***in*-[3-Cl]$^{2+}$**) and CCDC-1950947 (***in*-[3-CH$_3$CN]$^{3+}$**) contain the supplementary crystallographic data for this paper. The data for these structures can be obtained free of charge from the Cambridge Crystallographic Data Centre *via* www.ccdc.cam.ac.uk/data_request/cif.

4. Conclusions

We have prepared a new Ru dyad molecule in which one metal of the dinuclear complex acts as a light harvester and the other as a catalyst. We have thoroughly characterized the new complex spectroscopically and electrochemically. In addition, we have shown that a variety of organic substrates, such as alcohols, alkenes, and sulfides can be selectively photocatalytically oxidized by the dyad. The mechanism of action of the light induced oxidation of these organic substrates using a chromophore-catalyst system such as the one discussed in this paper has been previously discussed.[22,23,33] But by comparing to similar systems, we have shown that by tuning the electronic coupling between the Ru_pRu_c we can significantly alter the catalytic activity of the molecule.

The future outlook on these complexes will be the need to determine the method of intramolecular energy transfer in the molecule. This energy transfer between similarly structured Ru centres has been the topic of discussion in other theoretical research.[15] This will also be carried out alongside calculations on the electron transfer rates of the shuttling between the two metal centers to further optimize the catalytic activity of the dyads.

Conflicts of interest

There are no conflicts to declare.

Acknowledgements

Support from MINECO (CTQ2010-21497), Generalitat de Catalunya, and "la Caixa" Foundation are gratefully acknowledged. SH acknowledges support from College of Science scholarship, NUI Galway. PF acknowledges support from Royal Society Newton Alumni programme.

Notes and References

1 N. Armaroli and V. Balzani, *Angew. Chemie - Int. Ed.*, 2007, **46**, 52–66.

2 V. Balzani, A. Credi and M. Venturi, *Photochemical conversion of solar energy*, 2008, vol. 1.

3 D. G. Nocera, *Acc. Chem. Res.*, 2017, **50**, 616–619.

4 S. Hennessey and P. Farràs, *Chem. Commun.*, 2018, **54**, 6662–6680.

5 P. Garrido-Barros, I. Funes-Ardoiz, P. Farràs, C. Gimbert-Suriñach, F. Maseras and A. Llobet, in *Catalytic Oxidation in Organic Synthesis*, 2017, pp. 63–79.

6 M. Hajimohammadi, N. Safari, H. Mofakham and F. Deyhimi, *Green Chem.*, 2011, **13**, 991–997.

7 D. Kalita, B. Radaram, B. Brooks, P. P. Kannam and X. Zhao, *ChemCatChem*, 2011, **3**, 571–573.

8 M. D. Kärkäs, O. Verho, E. V. Johnston and B. Åkermark, *Chem. Rev.*, 2014, **114**, 11863–12001.

9 N. Kaveevivitchai, R. Chitta, R. Zong, M. El Ojaimi and R. P. Thummel, *J. Am. Chem. Soc.*, 2012, **134**, 10721–10724.

10 P. Farràs, S. Maji, J. Benet-Buchholz and A. Llobet, *Chem. Eur. J.*, 2013, **19**, 7162–7172.

11 P. Guillo, O. Hamelin, P. Batat, G. Jonusauskas, N. D. McClenaghan and S. Ménage, *Inorg. Chem.*, 2012, **51**, 2222–2230.

12 W. Iali, P. H. Lanoe, S. Torelli, D. Jouvenot, F. Loiseau, C. Lebrun, O. Hamelin and S. Ménage, *Angew. Chemie - Int. Ed.*, 2015, **54**, 8415–8419.

13 P. Farràs and A. C. Benniston, *Tetrahedron Lett.*, 2014, **55**, 7011–7014.

14 A. Haim, *Acc. Chem. Res.*, 1975, **8**, 264–272.

15 E. Jakubikova, R. L. Martin and E. R. Batista, *Inorg. Chem.*, 2010, **49**, 2975–2982.

16 W. R. Browne, R. Hage and J. G. Vos, *Coord. Chem. Rev.*, 2006, **250**, 1653–1668.

17 M. Parthey and M. Kaupp, *Chem. Soc. Rev.*, 2014, **43**, 5067–5088.

18 P. Farràs, C. Di Giovanni, J. N. Clifford, E. Palomares and A. Llobet, *Coord. Chem. Rev.*, 2015, **304**–**305**, 202–208.

19 M. R. Norris, J. J. Concepcion, D. P. Harrison, R. A. Binstead, D. L. Ashford, Z. Fang, J. L. Templeton and T. J. Meyer, *J. Am. Chem. Soc.*, 2013, **135**, 2080–2083.

20 W. Chen, F. N. Rein, B. L. Scott and R. C. Rocha, *Chem. Eur. J.*, 2011, **17**, 5595–5604.

21 J. A. Treadway, J. A. Moss and T. J. Meyer, *Inorg. Chem.*, 2002, **38**, 4386–4387.

22 O. Hamelin, P. Guillo, F. Loiseau, M. F. Boissonnet and S. Ménage, *Inorg. Chem.*, 2011, **50**, 7952–7954.

23 K. Senthil Murugan, T. Rajendran, G. Balakrishnan, M. Ganesan, V. K. Sivasubramanian, J. Sankar, A. Ilangovan, P. Ramamurthy and S. Rajagopal, *J. Phys. Chem. A*, 2014, **118**, 4451–4463.

24 S. Phungsripheng, K. Kozawa, M. Akita and A. Inagaki, *Inorg. Chem.*, 2016, **55**, 3750–3758.

25 F. Nastasi, A. Santoro, S. Serroni, S. Campagna, N. Kaveevivitchai and R. P. Thummel, *Photochem. Photobiol. Sci.*, 2019, **18**, 2164–2173.

26 C. Sens, M. Rodríguez, I. Romero, A. Llobet, T. Parella and J. Benet-Buchholz, *Inorg. Chem.*, 2003, **42**, 8385–8394.

27 W. Zhang, J.-H. Liu, J.-X. Pan, P. Li and L.-C. Sun, *Polyhedron*, 2008, **27**, 1168–1176.

28 X. Sala, E. Plantalech, I. Romero, M. Rodríguez, A. Llobet, A. Poater, M. Duran, M. Solà, S. Jansat, M. Gómez, T. Parella, H. Stoeckli-Evans and J. Benet-Buchholz, *Chem. Eur. J.*, 2006, **12**, 2798–2807.

29 C. Sens, I. Romero, M. Rodríguez, A. Llobet, T. Parella and J. Benet-Buchholz, *J. Am. Chem. Soc.*, 2004, **126**, 7798–7799.

30 J.-P. Launay and M. Verdaguer, *Electrons in molecules: From basic principles to molecular electronics*, 2014.

31 K. D. Demadis, C. M. Hartshorn and T. J. Meyer, *Chem. Rev.*, 2001, **101**, 2655–2685.

32 S. Roeser, M. Z. Ertem, C. Cady, R. Lomoth, J. Benet-Buchholz, L. Hammarström, B.

Sarkar, W. Kaim, C. J. Cramer and A. Llobet, *Inorg. Chem.*, 2012, **51**, 320–327.

33 T. T. Li, F. M. Li, W. L. Zhao, Y. H. Tian, Y. Chen, R. Cai and W. F. Fu, *Inorg. Chem.*, 2015, **54**, 183–191.

34 C. Dowling, D. R. Dinsdale and M. T. Lemaire, *Can. J. Chem.*, 2015, **93**, 769–774.

35 D. J. Wasylenko, C. Ganesamoorthy, B. D. Koivisto, M. A. Henderson and C. P. Berlinguette, *Inorg. Chem.*, 2010, **49**, 2202–2209.

36 B. P. Sullivan, D. J. Salmon and T. J. Meyer, *Inorg. Chem.*, 1978, **17**, 3334–3341.

37 M. J. Frisch, G. W. Trucks, H. B. Schlegel, G. E. Scuseria, M. A. Robb, J. R. Cheeseman, G. Scalmani, V. Barone, G. A. Petersson, H. Nakatsuji, X. Li, M. Caricato, A. V. Marenich, J. Bloino, B. G. Janesko, R. Gomperts, B. Mennucci and D. J. Hratch, 2016, Gaussian 16, Revision C.01.

38 Y. Zhao and D. G. Truhlar, *Theor. Chem. Acc.*, 2008, **120**, 215–241.

39 J. P. Perdew, K. Burke and M. Ernzerhof, *Phys. Rev. Lett.*, 1996, **77**, 3865–3868.

40 J. M. L. Martin and A. Sundermann, *J. Chem. Phys.*, 2001, **114**, 3408–3420.

41 D. Andrae, U. Haußermann, M. Dolg, H. Stoll and H. Preuß, *Theor. Chim. Acta*, 1990, **77**, 123–141.

42 *Data collection with APEX II versions v1.0–22, v2009.1–0 and v2009.1–02. Bruker, 2007. Bruker AXS Inc., Madison, Wisconsin, USA*, 2007.

43 *Data reduction with Bruker SAINT versions V.2.10, 2003, V/.60 A and V7.60 A. Bruker, 2007. Bruker AXS Inc., Madison, Wisconsin, USA*, 2003.

44 *SADABS: V.2.10, 2003; V2008 and V2008/1 Bruker, 2001, Bruker AXS Inc., Madison, Wisconsin, USA; R. H. Blessing, Acta Crystal- logr. Sect. A 1995, 51, 33–38.*, 2003.

45 SHELXTL versions V6.12 and 6.14; G. M. Sheldrick, *Acta Crystal- logr. Sect. A*, 2008, 64, 112–122.